A More Precise Algorithm to Account for Non Concentric Multibeam Array Geometry

Travis Hamilton[1,3], Jonathan Beaudoin[2], John Hughes Clarke[1]

1: Ocean Mapping Group, University of New Brunswick
2: Center for Coastal and Ocean Mapping, University of New Hampshire
3: UTEC Survey

Abstract

While the offset between transmitter and receiver acoustic centres has always been known, previously published algorithms for multibeam ray tracing assume a virtual concentric array geometry. The simplification permits the estimation of a single beam vector for launch and return. To fully accommodate the offset would require acknowledging the separation of the two refracted ray paths. For single sector systems the consequences are typically negligible, however due to pronounced transmit steering in multi-sector systems, the biases that result in post-processing are larger and show up as discrete steps at sector boundaries. Currently only a proprietary algorithm is available with these systems that preclude third party recalculation.

A more precise algorithm has been developed which now accounts for the separation between transmit and receive arrays. The algorithm models the intersection of two non-concentric cones with the seabed by intersecting hyperbolas on a plane at a defined depth. Through an iterative process a best estimate of the depth is reached, at which point the non-equal partitioning of the travel time is achieved and two vectors, one from each array, are derived. Using one of the two travel times and its corresponding vector, a geographic location for each sounding is then calculated using traditional ray tracing methods, however, now with a beam launch angle and travel time that respect the true bi-static nature of the sonar configuration.

An example multi-sector dataset is processed using both the new and old algorithms, demonstrating how the newly developed algorithm allows the correction of data artifacts associated with previous algorithms.

1 Introduction

During a multibeam echosounder (MBES) survey there are multiple types of observations that contribute to the final geographic location for each sounding. These observations include mount location and angles of the transmit and receive arrays in the vessel reference frame, sound speed structure of the water column, orientation and position of the vessel, array relative beam steering angles for transmit and receive beams, surface sound speed, and the two way travel time (twtt) [Lurton, 2010]. MBES systems and/or acquisition systems use their own algorithms in real-time to deliver the sounding solutions, however if any of the observations are externally logged or are erroneous and can be corrected, the need to re-integrate all the observations into a final sounding position in post-processing may arise.

The currently published algorithm used to re-integrate MBES data (cone intersection algorithm) is described in detail by *Beaudoin and Hughes Clarke (2004a)*. The drawback of the algorithm is that it assumes the transmit (TX) array at time of transmission, and the receive (RX) array at time of reception are co-located [Beaudoin et al, 2004b]. They recognized that the separation between transmitter and receiver is being ignored, and that this assumption may introduce biases into the soundings [Beaudoin et al, 2004b]. It was noted that "While the errors incurred are negligible in deep water, future work should focus on modeling the intersection of non-concentric cones such that the model more correctly represents reality in the case of shallow water soundings" [Beaudoin et al, 2004b]. The co-location assumption simplifies the mathematics but the fact remains that it does introduce errors into the final sounding positions.

The co-located array biases are exacerbated by the larger array separations introduced by narrow beam MBES systems. In addition, with the introduction of multi-sector MBES systems, multiple transmit beams can be steered fore and aft, also resulting in the size of the biases growing. With the introduction of multi-sector, narrow beam systems the biases can now be large enough to have visibly negative effects on the final products produced from MBES surveys, thus creating a need for new processing methodologies to be developed.

Although the Ocean Mapping Group has been re-processing shallow water soundings over the years, the majority of the soundings have been from an EM3002, which has both arrays mounted inside a 33.2 cm diameter cylinder [Kongsberg, 2006], imposing a minimal separation between the arrays. In addition the EM3002 is a single sector system, resulting in no abrupt changes in transmit steering making the biases appear consistent across the swath. The biases did not become evident until shallow water programs began with the EM710, EM302, and EM2040, which are multi sector, yaw stabilized, large array systems. The EM710/EM302 systems have much larger array separations (on the magnitude of metres) than the EM3002, and have multiple transmit sectors which are steered as much as +/- 10° in order to accommodate pitch and yaw stabilization [Personal communication with Kongsberg engineers]. All of these factors have combined together to create biases that are proving to be detrimental to post-processing efforts (Figure 1).

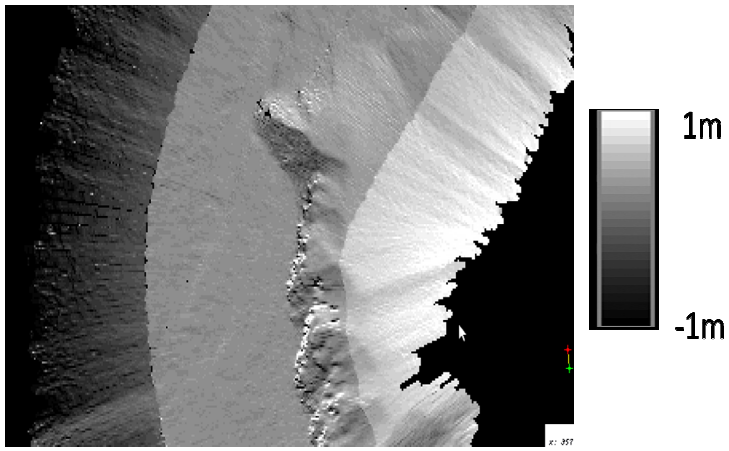

Figure 1: Difference map between data as collected, and data re-processed with the cone intersection algorithm. Soundings from an EM710 in depths of 150m to 200m (biases are 0.5%-0.7% w.d.).

There are two ways in which a separation between the arrays is introduced. The first is the arrays are mounted in physically separate locations on the vessel (Figure 2), and is a fixed value. The second separation comes from the forward propagation of the vessel during the transmit/receive cycle, this being the product of the vessel's velocity and a particular sounding's twtt. Since the twtt increases with water depth, the second separation is dynamic and grows as water depth increases. A more precise algorithm has been developed which allows the separation between arrays to be accounted for while re-integrating the MBES data. The new algorithm receives the fixed separation and calculates the dynamic separation, allowing an estimate of the sounding position, which is significantly improved from the estimate of the current algorithm, to be calculated.

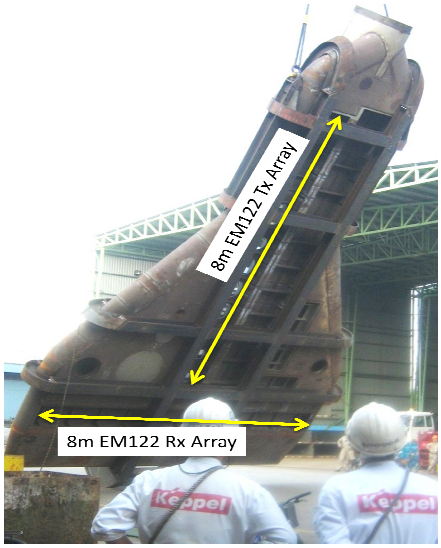

Figure 2: Gondola of the USNS Heezen. It houses an EM122 among other instruments

2 Background

Each beam of a multibeam echosounder is formed where the projection of the transmit cone on the seabed, and the projection of the receive cone on the seabed intersect. The location of a sounding is, in theory, the intersection of the two cones which form the transmit and receive beams, with a plane representing the seabed (Figure 3). However, in reality the sound travels along a refracting path through the water-column [Lurton, 2010], so the cone shape only holds true in defining a range of directions (fixed opening angle, but any potential angle about the cone) in which the beam can initially leave the TX array, and a range of directions in which it can return into the RX array. In order to know the location of each sounding, we must calculate one of these directions (will only discuss the direction from the TX array as both directions point to the same location), then we are able to ray trace using the direction and a travel time.

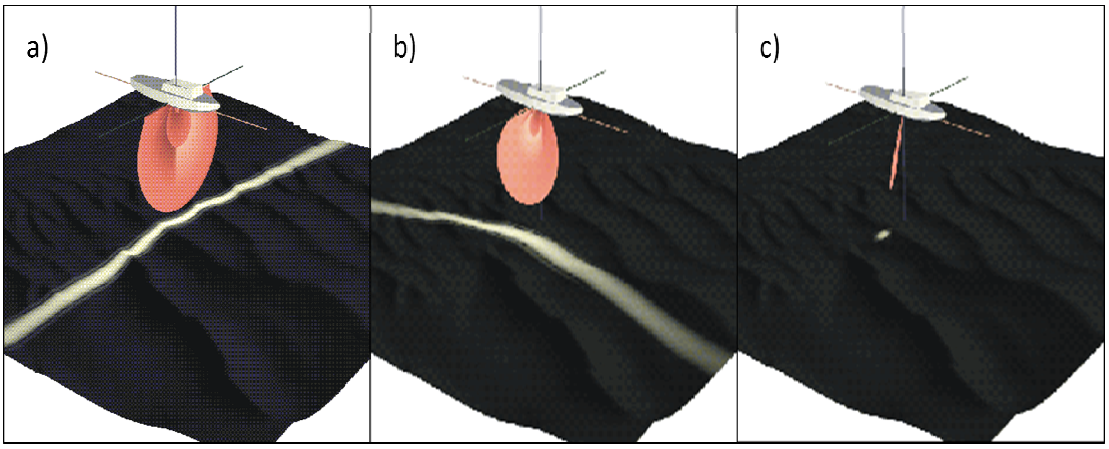

Figure 3: a) Cone shaped transmit beam pattern being projected onto the seabed. b) Cone shaped receive beam pattern being projected onto the seabed. c) Intersection of the two beam patterns on the seabed form the location of the sounding.

There are two conic parameters required to define the direction a beam leaves the TX array, they are the opening angle of the cone, and the angle about that cone. The opening angle of the cone is equal to the array relative beam steering angle subtracted from 90°, with the beam steering angle being a known value. The only unknown that remains is the angle about the cone. With two cones that do not share a vertex, the angle about each cone which points to where the intersection point is varies as you travel away from their vertices. Relating that to multibeam geometry, as the depth of the seabed below the multibeam sonar increases, the direction at which the beam leaves the transmit array changes (Figure 4), asymptotically approaching the value that would be calculated with the co-located assumption. In order to correctly determine the direction in which the beam leaves the transmit array the depth of the seabed below the array must be known, but in order to know the depth a direction and one way travel time (owtt) (which is a depth dependant fraction of the measured twtt) are required, creating an interdependency. The interdependency creates a complex, non-analytical, geometric problem.

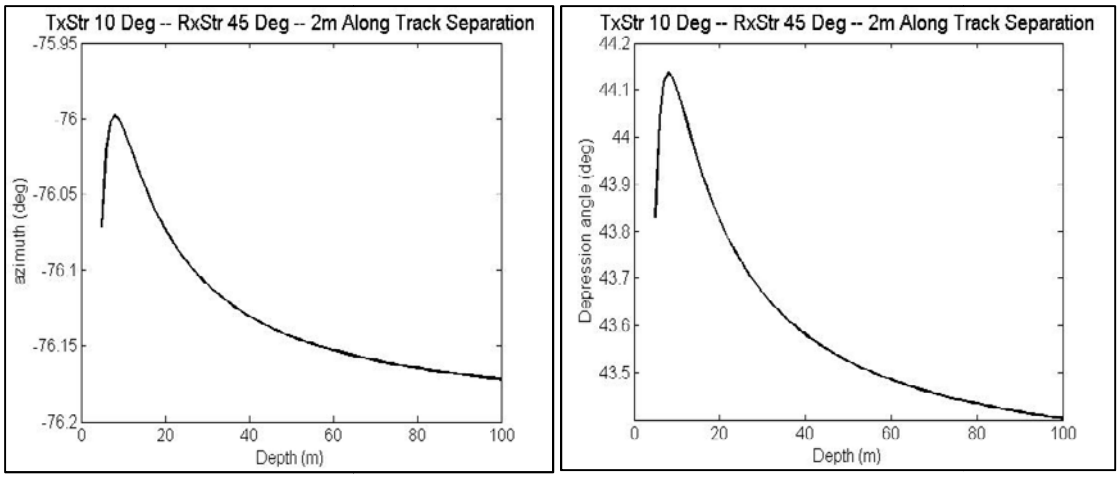

Figure 4: For a fixed set of steering angles and separation between arrays, the direction at which the beam leaves the TX array varies with depth (direction is depth dependant). Left panel shows the azimuth, right panel shows the depression angle.

To avoid dealing with the complexities of calculating the location of a sounding using the true sounding geometry, the cone intersection algorithm introduces an assumption that the TX and RX arrays are co-located [Beaudoin et al, 2004b]. With a co-location assumption the beam is forced to travel along the same path from the TX array to the seabed as it does from the seabed to the RX array. As the beam travels the same path in both directions, and that path is constrained by a vertical plane, the depression angle and azimuth are depth independent, and the travel time is always partitioned into two equal segments (Figure 5). The co-located array assumption converts a non-analytical problem into a depth independent analytical problem.

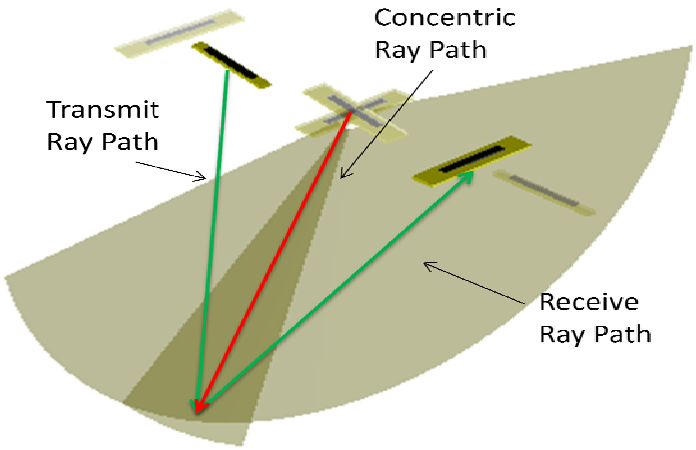

Figure 5: Green lines represent the true ray path, while the red line represents the calculated ray path when using a co-located array assumption. Transmit and receive ray paths are not necessarily of equal length.

The co-location assumption causes biases in along track, across track, and depth positions of each sounding. When the two arrays are assumed to be co-located, the location of the receive beam footprint is translated on the seafloor resulting in the calculated intersection point, of the two beam patterns with the seafloor, to be shifted away from its true location (Figure 6a). The range of the ray path from the arrays to the intersection point is a fixed value, thus when the intersection point moves in the along track or across track direction, it also moves vertically resulting in biases in all three coordinates (Figure 6c).

The magnitude of the biases are greatly influenced by the amount of transmit and receive steering. The intersection of a cone (the three dimensional shape that the beam forms when steered) and a plane (the seafloor) is a hyperbola (the beam footprint on the seafloor). As the steering angle of a beam increases, so does the eccentricity of the resulting hyperbola, which results in a larger across track versus along track slope on the hyperbola. The larger slope results in a larger across track offset between the true and calculated intersection points from an along track translation of the beam footprint, and vice versa. In addition to the increase in eccentricity, a larger transmit steering angle pushes the intersection point away from the vertex of the receiver beam footprint, into the area of higher slope (Figure 6b).

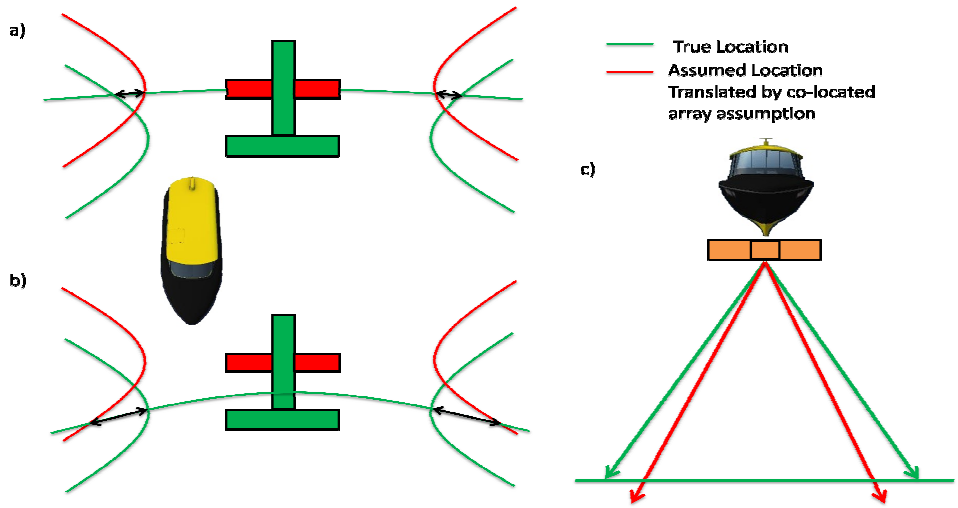

Figure 6: a) By assuming the transmit and receive arrays are co-located, an incorrect intersection point is calculated. b) With increased transmit beam steering, the difference between true and assumed intersection points is maximized. c) Ray has same length but different direction, causing an error in depth.

3 Methodology

Initially the research direction was focused on attempting to rigorously model the true geometry under which the transmitter beam pattern, receiver beam pattern and seafloor intersect. It was proving to be a successful endeavour up until the final step of raytracing was introduced. In order to ray-trace, the beam must be represented by an azimuth and depression angle, along with a owtt. When the two cones are not co-located, the ability to calculate a single depression angle and azimuth to represent the beam's direction is no longer feasible. It is not just a simple matter of having two pairs of azimuths and depression angles either, there is also a need to determine which portion of the total twtt belongs to the transmit travel time, and which portion belongs to the receive travel time. The 6 values (TX-seabed travel time, seabed-RX travel time, TX azimuth, TX depression, RX azimuth, RX depression) are all a function of the intersection point, however to accurately calculate an intersection point the ray-trace must be done.

The most complete approach to solve the problem would be to iterate through the range of possible launch vectors and receive vectors (launch vector is from the TX array and receive vector is from the RX array) as well as the possible divisions of the twtt, ray tracing each combination until the intersecting set of values was found. The issue is that this brute-force algorithm would be computationally expensive, putting limitations on the amount of survey data that would be feasible to re-process.

As a result of the computational cost associated with a brute-force algorithm, an assumption had to be found which improved upon the performance of the co-located array assumption, without introducing any significant biases of its own. Section 3.1 will outline the new algorithm, and the assumption which was introduced is addressed in Section 3.2.

3.1 Development Overview

The current cone intersection algorithm receives 14 angles;

- orientation of the vessel at time of transmission and reception (6 angles),
- mount angles of the TX and RX arrays (6 angles),
- TX beam steering (1 angle),
- and RX beam steering (1 angle),

as input and calculates the azimuth and depression angle that represents the direction the beam left the face of the co-located arrays [Beaudoin et al, 2004b]. The azimuth, depression angle, owtt and depth of the sonar are then used as inputs to a ray-tracing algorithm. The ray-trace algorithm computes the path the beam follows through the varying sound speed structure of the water column, allowing a transducer relative across track, along track, and depth for the sounding to be calculated [Lurton, 2010]. The final step is to then reduce the sounding coordinates back to the vessel reference point [Beaudoin et al, 2004b].

For ease of implementation, the new algorithm is designed to fit into the existing code structure while making the fewest possible changes (Figure 7). In order to achieve this, the new algorithm only replaces the calculation of the geographic azimuth and depression angle, and in addition must also partition the twtt into two unequal segments. The result is an algorithm which is designed to receive the same 14 angles, along with the 3D linear offsets between the arrays and the vessel velocity. The new algorithm then returns the geographic azimuth and depression angle which represent the direction the beam leaves the face of the TX array, and the owtt from the TX array to the seabed. Doing so allows the components of the previous algorithm that ray trace and reduce the sounding back to the reference point to remain unchanged.

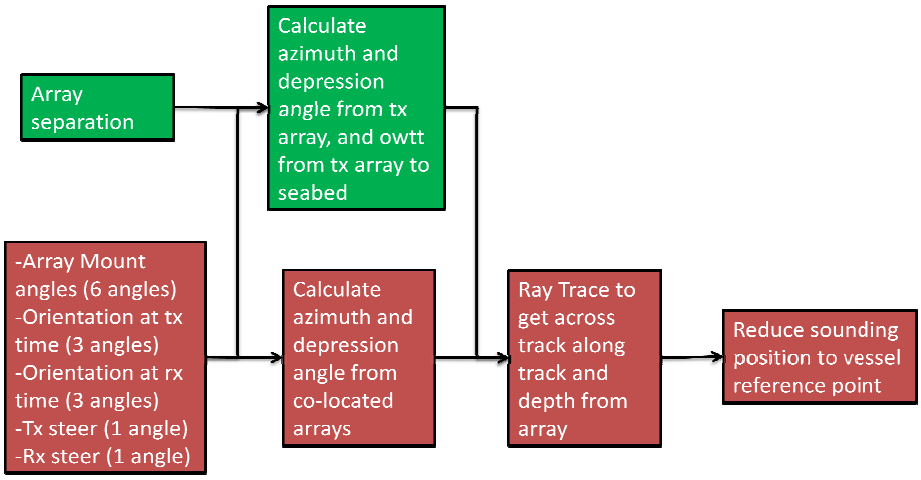

Figure 7: Flow chart demonstrating the steps required to integrate multibeam echosounder observations. Red represents the current method, and green shows were the improvements will be implemented.

Section 2 explained how, in order to reproduce the true direction in which the sounding left the transmit array, we must solve the non-analytical three dimensional problem of intersecting two non-concentric cones with a plane representing the seabed. An algorithm has been developed that achieves a very close approximation to this, but it does so by breaking down the three dimensional problem to a two dimensional problem of intersecting hyperbolas. It is known that the beam leaves the TX array on a cone defined by the TX steering angle; the unknown is the angle about that cone (Figure 8a). By intersecting the two hyperbolas, one for each the TX cone's and the RX cone's intersection with a plane at a iteratively resolved focal range, the angle about the TX cone can be calculated, defining the beam launch vector (Figure 8b). Once the beam launch vector is known the beam's azimuth and depression angle can be calculated, and the beam can be ray traced to produce its final sounding coordinates. It is only a close approximation because as the cones refract through the non-homogenous water-column they no longer form perfect hyperbolas upon intersecting a plane. This issue is discussed in Section 3.2.

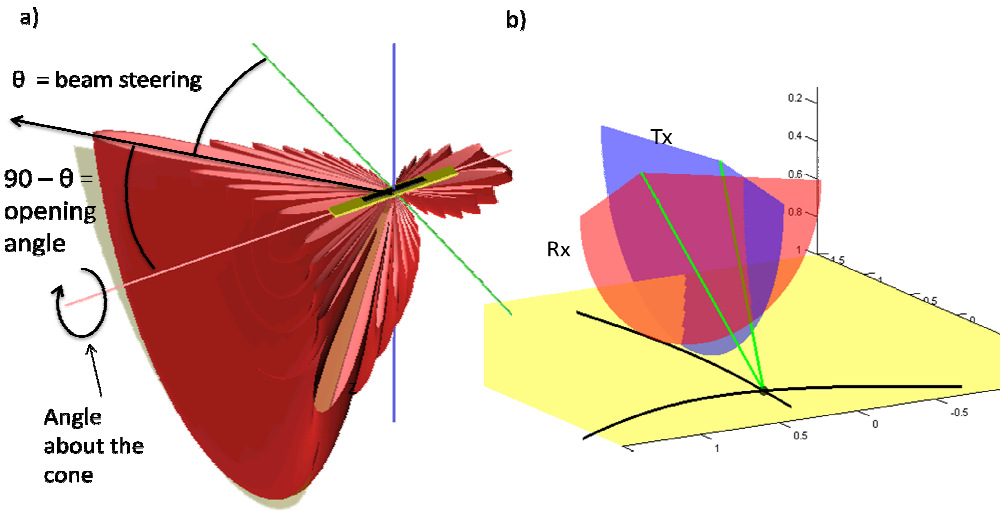

Figure 8: a) Must solve for the angle about the cone to be able to calculate launch and receive vectors. b) Intersect hyperbolas on the focal plane to solve for the angle about each cone.

There are 6 major steps in the new algorithm. The steps will be explained with detail throughout this section and are as follows:

1. Define the array-relative reference frame.
2. Calculate the 3-Dimensional array separation in the reference frame from (1).
3. Calculate the initial estimate of the Focal Range.
4. Define and intersect the two hyperbolas on a plane at distance informed by (3).
5. Calculate the TWTT required to get to the intersection point from (4).
6. Adjust estimate of Focal Range based on the difference between calculated TWTT from (5) and the measured TWTT. Repeat from step 4.

3.1.1 Array Relative Reference Frame

In order to define and intersect the hyperbolas (Section 3.1.4), an array relative reference frame (ARF) must be defined. The ARF is defined in the same way as it is for the current cone intersection algorithm, and the formulas can be found in *Beaudoin 2004a*. Even though the formulas for defining the ARF are the same for the two algorithms, the results of the reference frame definition differ slightly. Table 1 outlines these differences.

	Current Algorithm	**New Algorithm**
Tx array centre	N/A	Origin of reference frame
Rx array centre	N/A	Coordinates = 3D array offset
Co-located arrays centre	Origin of reference frame	N/A
Tx array orientation	Aligned with X-axis	Aligned with X-axis
Rx array orientation	Parallel to X/Y plane	Parallel to X/Y plane

Table 1: Array Reference Frame definition.

To elaborate on Table 1, the ARF is designed so the TX array at time of transmission is the origin, and the X/Y plane is parallel to the TX array at time of transmission and the RX array at time of reception. The two major changes to the definition of the ARF for the new method are; that the RX array is parallel the X/Y plane but not located on it, and the origin is at the centre of the TX array at time of transmission.

As outlined in *Beaudoin and Hughes Clarke (2004a)*, the ARF is a right-handed coordinate system, and its axes are defined relative to the vessel reference frame (VRF) (X-axis forward, Y-axis starboard, Z-axis down). As a result the unit vectors representing to X, Y and Z axis of the ARF frame within the VRF can be used to form a rotation matrix ($R_{geo)}$ which can convert vectors back into the VRF, and the transpose of R_{geo} can convert vectors from the VRF into the ARF. R_{geo} is defined by equation 1 [Beaudoin and Hughes Clarke, 2004a].

$$R_{geo} = \begin{bmatrix} X_x^{ARF} & Y_x^{ARF} & Z_x^{ARF} \\ X_y^{ARF} & Y_y^{ARF} & Z_y^{ARF} \\ X_z^{ARF} & Y_z^{ARF} & Z_z^{ARF} \end{bmatrix}. \quad (1)$$

The reason for needing to define and intersect the hyperbolas within the ARF is due to the principals of conics. A hyperbola is formed when a cone intersects a plane which is oriented at an angle, relative to the central axis of the cone, which is less than the opening angle of that cone (Figure 9). If the calculations were done in the VRF there could be scenarios, based on the differing orientations and steering angles of the TX and RX cones, where the intersection would form a parabola rather than a hyperbola. By performing the calculations in the ARF, the central axis of the TX and RX cones will always be parallel to the focal plane on which they are being intersected (so they will both be hyperbolas).

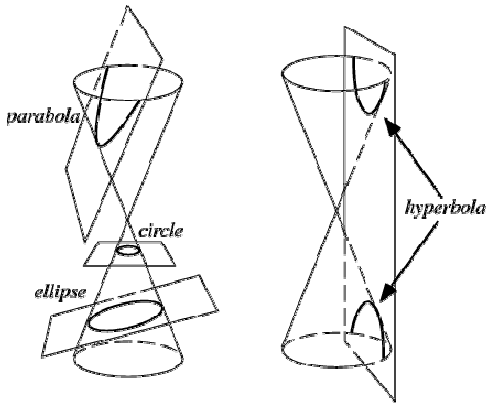

Figure 9: Conic sections. *Image courtesy of http://mathworld.wolfram.com/ConicSection.html*

An additional advantage to using the ARF is the TX array will be centered at the origin, and aligned with the X-axis. The result of this configuration is that it allows the TX hyperbola to be defined by the basic formula for a hyperbola (equations 11 through 14). Also the RX array is parallel to the X-Y plane, so it eliminates the need to rotate the RX array about the X or Y axis.

3.1.2 3-Dimensional Array Separation

There are two mechanisms through which the 3-Dimensional array separation is formed. The first is the static component, which is a result of the physical mounting of the arrays on a vessel. The static component varies between installations, but will always remain constant (within the VRF) for the duration of a survey. The second component is dynamic, and changes for each individual beam within a single ping. The dynamic component is caused by the movement of the vessel over the transmit/receive cycle. The TX cone will remain fixed in geographic space while the location of each RX cone will move (and potentially rotate) based on the vessel's velocity vector and that beam's twtt. As a result the dynamic component will grow as the twtt increases, which means it is larger for outer beams and for deeper water.

Calculating the 3-dimensional array separation is a three step process. The first step is to calculate the movement of the RX array within the geographic reference frame, between the time of transmission and the time of reception. The calculation is done using the vessel's positioning information along with vessel motion and the array's lever arm. The second step is rotating the dynamic separation from the geographic reference frame into the VRF using the vessel's heading. Finally, the third step is to combine the dynamic and static separations and rotate into the ARF using R_{geo}. The equations associated with calculating the 3-Dimensional separation are intentionally left out as they are standard geometry and geodesy calculations, and will vary depending on the geographic reference frame in use.

3.1.3 Initial Estimation of the Focal Range

As described in Section 2, a sounding is located where the TX cone, RX Cone and seabed intersect. For the new algorithm, rather than solving the 3-Dimensional intersection of two cones with the seabed, two hyperbolas (which represent the intersection of a cone with a plane) are

being intersected on the focal plane (a plane with strictly a Z-offset from the X-Y plane of the ARF) (Figure 10). The terms focal plane and focal range were chosen because an iterative process will be used to slide the focal plane back and forth until the correct focal range is found. Since an iterative approach is being used, there must be an initial estimate.

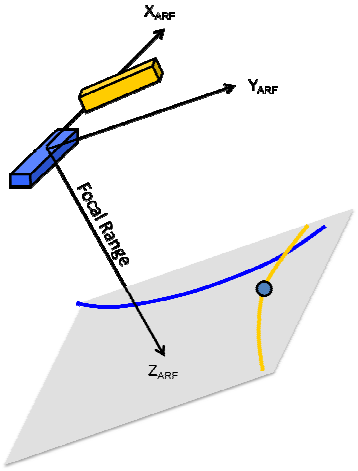

Figure 10: Hyperbolas are intersected on the focal plane, which is parallel to the X-Y plane of the ARF. Need to solve for the correct focal range.

The following sections will explain how intersecting the hyperbolas on the focal plane, at some arbitrary range permits an iterative process to begin, a process that results in finding the correct focal range which produces a calculated twtt equal to the measured twtt. Once that appropriate focal range is determined, the beam's launch and receive vectors can be calculated, and the twtt can be properly partitioned into a transmit owtt, and a receive owtt.

It is important to have a reasonable initial estimate of the focal range to allow the correct solution to be determined in the fewest possible iterations. The initial estimate is based off a rough approximation of the seafloor depth, which is calculated by assuming the beam launch vector (in the ARF) is based solely on the receive beam steering angle, and dividing the TWTT by 2. Equations 2 through 5 demonstrate the calculations.

$$\begin{bmatrix} X \\ Y \\ Z \end{bmatrix}_{VRF} = R_{geo} * \begin{bmatrix} 0 \\ \sin(-RxSteer) \\ \cos(-RxSteer) \end{bmatrix}, \quad (2)$$

$$Azimuth = atan2\,(Y, X)\ , \quad (3)$$

$$Depression\ Angle = atan\{Z/\sqrt{(X^2 + Y^2)}\}\ , \quad (4)$$

$$OWTT = TWTT\ /\ 2\ . \quad (5)$$

The next step is to ray trace based on the calculated Azimuth, Depression Angle, and OWTT. The initial estimate of depth is the value output from the ray trace. The final step is to then rotate the depth back into the ARF using the transpose of R_{geo}, which results in the focal range estimate used for intersecting the hyperbolas. The calculations result in a rough estimate of the focal

range, however it is a reasonable starting point which allows the correct range to be determined in very few iterations, typically 3 or 4.

3.1.4 Intersect the Hyperbolas

As described in Section 3.1.1, working in the ARF avoids overcomplicating the equations of the two hyperbolas. Working within the ARF means the x-axis is aligned with the TX array at time of transmission, and the X-Y plane is parallel to both the TX array at time of transmission, and the RX array at time of reception. As a result the transmit hyperbola takes the form of a horizontal transverse axis hyperbola, and the receive hyperbola is a vertical transverse axis hyperbola (Figure 11a). The receive hyperbola then requires only one rotation about the z-axis accounting for the non-orthogonality angle (δ in [Beaudoin et al, 2004b]), and a translation to account for the separation between the arrays (Figure 11b). The RX z-offset in the ARF is accommodated by allowing the RX hyperbola to scale independently of the TX hyperbola.

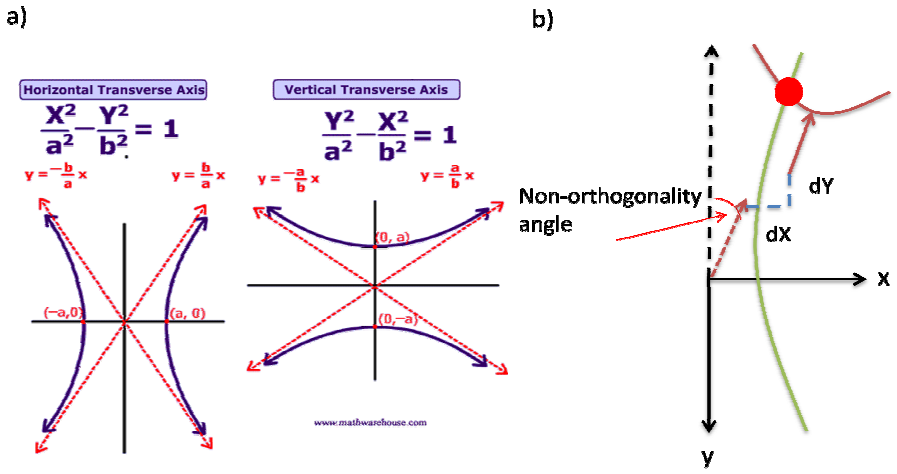

Figure 11: a) Different forms of a hyperbola. Left shows the horizontal transverse axis hyperbola (TX hyperbola). Right shows the vertical transverse axis hyperbola (RX hyperbola). *Image courtesy of www.mathwarehouse.com.* b) Receive hyperbola is rotated by non-orthogonality angle, and translated for array separation.

The shape of each hyperbola is defined by the constants *a* and *b* (Equations 6 & 7). They are a function of the array-relative steering angle (*TXsteer* and *RXsteer*) and the focal range (*R*) (Figure 12). As the hyperbolic intersection will occur on a plane of constant range, the Z offset of the RX array is taken into account when defining the shape of the RX hyperbola. The Z offset is accounted for by defining the shape of the RX hyperbola using a focal range which has been adjusted by the Z offset (Equations 8 through 12).

$$a_{tx} = R * \tan(TXsteer)\,, \quad (6)$$

$$b_{tx} = R\,, \quad (7)$$

$$R_{rx} = R - Dz\,, \quad (8)$$

$$a_{rx} = R_{rx} * \tan(-RXsteer)\,, \quad (9)$$

$$b_{rx} = R_{rx}\,. \quad (10)$$

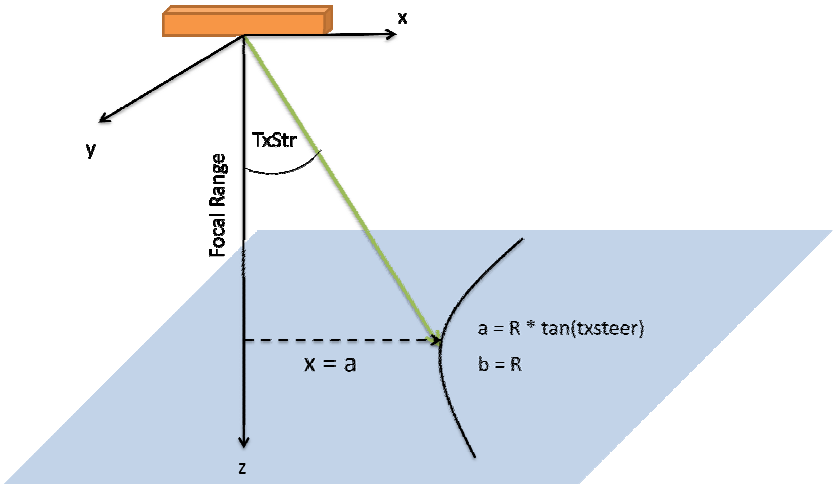

Figure 12: Definition of the shape of the TX hyperbola. The constants a and b for a hyperbola are dependent on the array relative beam steering angle, and the focal range (R).

In order to calculate the intersection of two hyperbolas, the parametric version of the equation of a hyperbola is used. Equations 11 and 12 form a horizontal transverse (TX) hyperbola, and equations 13 and 14 form a vertical transverse (RX) hyperbola:

$$x = a * \cosh(t1), \quad (11)$$
$$y = b * \sinh(t1), \quad (12)$$
$$x = b * \sinh(t2), \quad (13)$$
$$y = a * \cosh(t2). \quad (14)$$

The values *a* and *b* are the constants defined above, while *t1* and *t2* are the parametric variables, representing the angle about the transmit and receive cones respectfully. The RX hyperbola must be rotated about the z-axis and translated for the separation between arrays, thus the final form of its parameterized equations are Equations 15 and 16;

$$x = \cos(m) * b * \sinh(t2) - \sin(m) * a * \cosh(t2) + dX, \quad (15)$$
$$y = \sin(m) * b * \sinh(t2) + \cos(m) * a * \cosh(t2) + dY, \quad (16)$$

where *m* is the non-orthogonality angle. Finding the intersection point becomes a matter of solving a system of 4 equations (Equations 11,12,15,16) and 4 unknowns (*x,y,t1,t2*).

The system of 4 equations and 4 unknowns does not have an analytical solution, therefore Newton's Method of solving a system of equations is used [Bradie, 2006]. The Newton Method was chosen for its ability to find a solution with only a few number of iterations. The Newton method requires there to be a condition to determine if the current iteration of the solution is satisfactory. The condition chosen for the hyperbolic intersection is that the change in *x* and *y*, between the current and previous iterations, are 1mm or smaller. Using 1mm is small enough to

ensure the precision of the intersection point is high enough to avoid negative effects on the remainder of the calculations, while being large enough to prevent un-necessary iterations.

By differencing the intersection point with the array coordinates, the launch and receive vectors are formed and can be rotated back into the VRF (Equation 17 and 18). The two vectors can then be used to calculate the TX azimuth / depression angle, and the RX azimuth / depression angle (Equations 19 through 22).

$$\begin{bmatrix} X \\ Y \\ Z \end{bmatrix}_{TX} = R_{geo} * \begin{bmatrix} x \\ y \\ R \end{bmatrix}, \quad (17)$$

$$\begin{bmatrix} X \\ Y \\ Z \end{bmatrix}_{RX} = R_{geo} * \begin{bmatrix} x - Dx \\ y - Dy \\ R - Dz \end{bmatrix}, \quad (18)$$

$$Azimuth_{TX} = atan2\,(Y_{TX}, X_{TX}), \quad (19)$$

$$Depression\ Angle_{TX} = atan\{Z_{TX}/\sqrt{(X_{TX}^2 + Y_{TX}^2)}\ \}, \quad (20)$$

$$Azimuth_{RX} = atan2\,(Y_{RX}, X_{RX}), \quad (21)$$

$$Depression\ Angle_{RX} = atan\{Z_{RX}/\sqrt{(X_{RX}^2 + Y_{RX}^2)}\ \}. \quad (22)$$

3.1.5 Calculated TWTT

Having the direction that the beam leaves the transmit array, and the direction at which it returns to the receive array allows two separate modified ray-traces to be performed. Typically a ray-tracing algorithm uses the depression angle to launch a ray and follows its refracting path as a function of time through the water-column, stopping the computation when the computed time equals the measured time, returning a depth and horizontal distance for the sounding [Lurton, 2010]. The modified ray-trace uses a similar approach, however it follows the ray's path as a function of depth, stopping when the computed depth equals the depth associated with the intersection point, returning the time required for the ray to reach the depth of the intersection point. The depth is calculated by rotating the focal range into the VRF. The modified ray-trace allows a owtt from the TX array to the seabed, and a owtt from the seabed to the RX array to be calculated, which combined form the calculated twtt.

3.1.6 Adjust Focal Range

Once the calculated twtt is determined, it can be compared against the actual measured twtt, acting as an indicator of how the focal range needs to be changed for the next iteration of the hyperbola intersection. Both the magnitude and direction of the shift in range are calculated from the time difference, using Equation 23, where ss_{tx} is the sound speed at the current depth estimate.

$$Range\ Increment = \frac{twtt_{meas} - twtt_{calc}}{2} * ss_{tx} * \sin(dep_{tx}). \quad (23)$$

If the calculated twtt is longer than the measured twtt, the depth increment will be negative, causing a shallower depth for the next iteration. If the calculated twtt is shorter than the measured twtt, the depth increment will be positive, causing a deeper depth for the next iteration.

The process of intersecting the hyperbolas, calculating the two depression angles, and ray tracing to get a calculated twtt is repeated until the calculated twtt matches the measured twtt. As a result of finding the correct depth, the twtt has been partitioned while the azimuth and depression angle at which the beam leaves the transmit array is calculated. The values which get passed back into the ray-tracing algorithm to produce the final sounding coordinates are as follows:

- Azimuth, as calculated from the TX array for the current iteration
- Depression angle, as calculated from the TX array for the current iteration
- Owtt, as calculated from the TX array to the seabed for the current iteration.

3.2 Limitations of the New Algorithm

As described above, hyperbolas are intersected to define the launch and receive vectors for each beam. The hyperbolas are used to model the intersection of two cones, which represent the transmit and receive beam patterns, with a plane representing the seabed. In reality those cones refract as they travel through the water-column and thus do not actually form a hyperbola when they intersect the seabed. As a result the calculated launch and receive vectors, which will intersect at a depth producing the correct twtt, will only intersect in a homogenous water-column. The assumption which is made in the new algorithm is, when the calculated launch and receive vectors are ray-traced for the duration of their corresponding owtt, they will end up at the same location in 3-Dimensional space. This is reasonable as once exiting the two arrays, they travel in vertical planes at the beam azimuth and share common distortions as a function of depth.

The biases introduced by the assumption can be tested by actually ray-tracing the launch and receive vectors for the duration of their corresponding owtt, and differencing their end coordinates. Figure 13 shows the difference between ray-tracing from the TX array, and ray-tracing from the RX array. Figure 13 is a profile of all beams in 1 ping from an EM2040 which has its port sector steered forward 9.61 degrees, central sector is steered forward 2.10 degrees and starboard sector steered back 7.39 degrees in 50 m of water. For comparison with the original method, Figure 14 shows the difference between the same ping processed using the current cone intersection algorithm which has the co-location assumption, and the original data as processed by the MBES manufacturer's proprietary algorithm, thus displaying the biases introduced by the co-located array assumption. By comparing figures 13 and 14 it is evident that the biases caused by the hyperbolic intersection assumption are negligible when compared to the biases caused by the co-located array assumption. It is this improvement that justifies the use of the hyperbolic intersection assumption in the new algorithm.

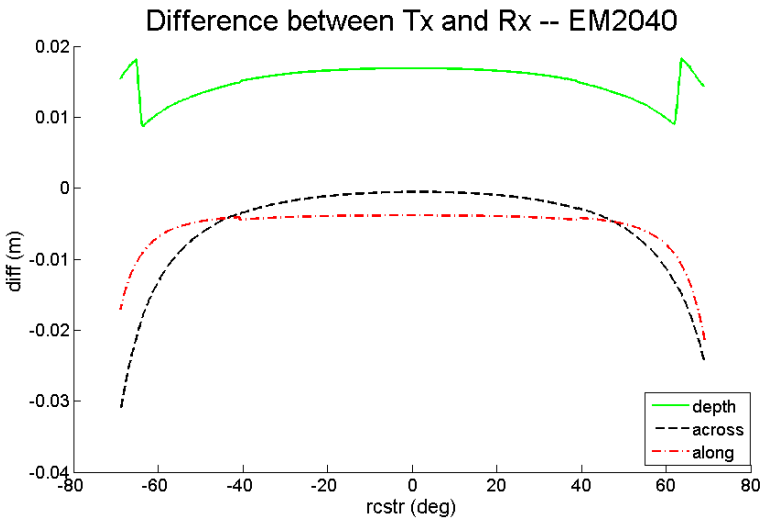

Figure 13: Difference between sounding coordinates calculated from the TX array, and sounding coordinates calculated from the RX array. Data is one ping from an EM2040.

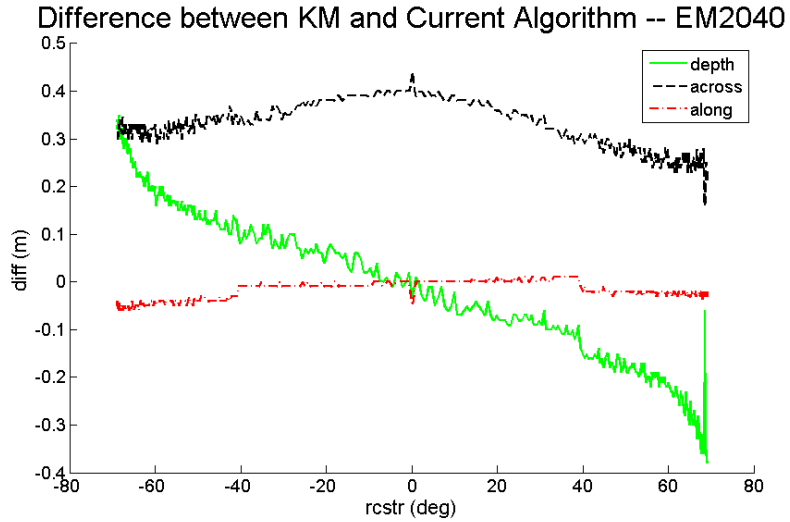

Figure 14: Difference between original data, and data re-integrated using the current cone intersection algorithm. Data is one ping from an EM2040. This image demonstrates the biases introduced by the co-location assumption.

It is possible to use hyperbolas because they are not being used to define the location of the sounding, rather they are being intersected to determine the angle about the TX and RX cones (*t1* and *t2*), and those angles are used to define the direction at which the beam left the TX array and returned to the RX array. That direction is then ray-traced through the water-column to get the actual sounding coordinate. In a scenario where the two arrays are actually co-located, the launch and receive vectors would be identical reducing the bias produced by the hyperbola assumption to zero. As the TX and RX arrays move away from each other, the difference between the incidence angle of the launch vector with the refracting layers, and the incidence angle of the receive vector with the refracting layers remains small. This results in the end point of the two

refracted ray-paths being close enough that the difference has a negligible effect on the final sounding coordinates. Several datasets have been tested, all showing similar improvements, however further work needs to be done to assure the assumptions holds up under all possible geometries.

4 Case Studies

4.1 Erroneous Array Mount Locations

A multibeam survey of a sand wave field off the coast of B.C. was performed in the spring of 2009. The survey was conducted using an EM710 which has the TX and RX arrays mounted in physically separate locations on the vessel. During the survey the mount locations of the arrays were incorrectly set within the sonar installation parameters. As a result, an incorrect separation between the arrays was used during the actual collection of the data, causing the sounding coordinates to be erroneous.

When the array mount locations are incorrectly set within the installation parameters, the biases introduced into the data will behave the same way as biases introduced by the co-located array assumption, which is explained in Section 2. As a result steps along the sector boundaries can be seen to grow as the ship is turning, due to increased transmit beam steering introduced for yaw stabilization (Figure 15). In order to fix the sector boundary steps in the survey all of the observations must be re-integrated in post processing, this time using the correct mount locations of the arrays within the vessel reference frame.

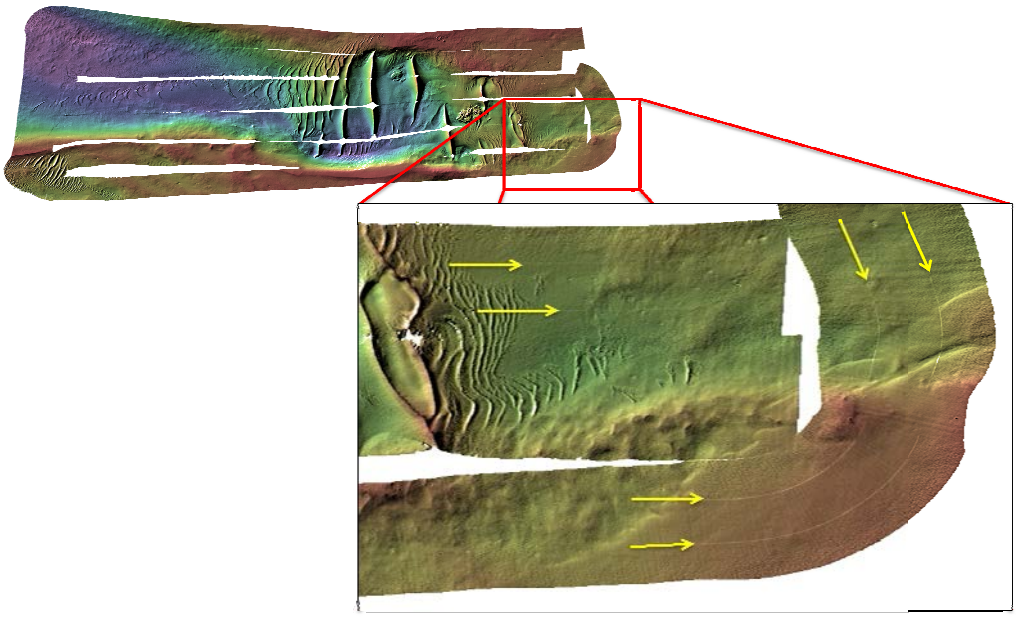

Figure 15: Sun illuminate, depth coloured grid of the survey as collected. Yellow arrows point to locations of sector boundary offsets which were caused by the erroneous array mount locations.

By changing the parameter file to accurately represent the true mount locations of the TX and RX arrays within the vessel reference frame, the data was able to be re-integrated using the new algorithm. Figure 16 points to locations where the sector boundaries were present in the original data. It can be seen that the artifacts caused by the incorrect mount locations have been removed from the data. When the data was reprocessed using the cone intersection algorithm, even though the true mount locations of the arrays were used, the co-location assumption created biases in the data which were nearly identical the original biases caused by the erroneous mount locations. This serves as a clear demonstration that the new algorithm has allowed an erroneous survey to be fixed, a task which could not previously be done.

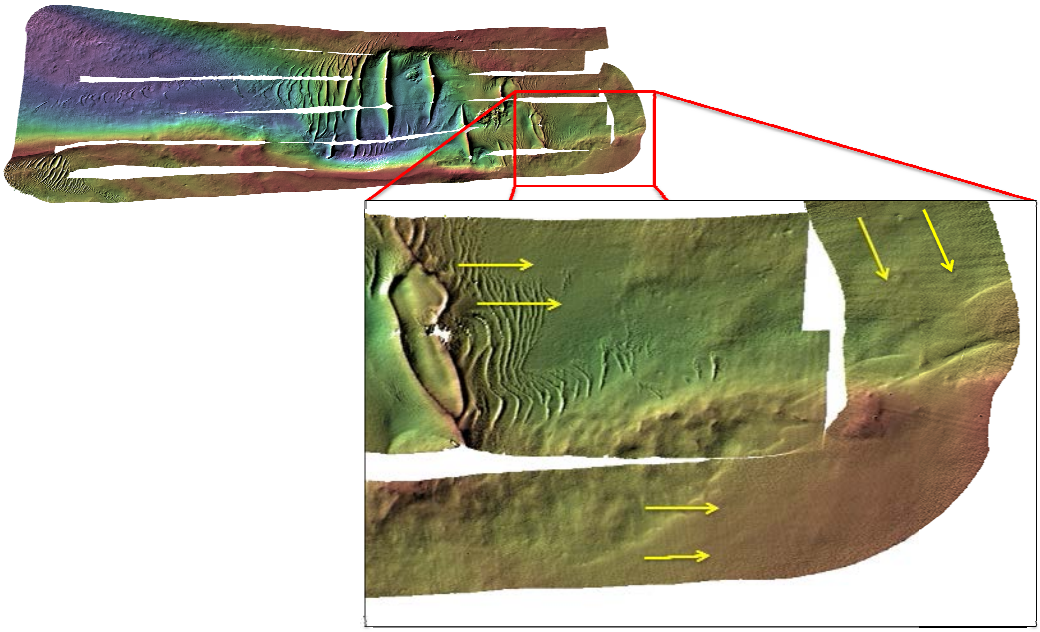

Figure 16: Sun illuminate, depth coloured grid of the survey reprocessed using the new algorithm and the correct array mount locations. Yellow arrows point to locations where the sector boundary steps no longer exist.

4.2 Application of New Sound Speed Profiles

In 2011, repeat multibeam surveys of the Squamish delta in British Columbia were performed with the goal of monitoring temporal seabed change on a decimetre scale [Hughes Clarke, 2012]. In order to achieve these results, the multibeam sonar and its ancillary systems had to be working at their peak levels. One of the ancillary systems was an ODIM Brooke Ocean MVP30, which is used to collect sound speed profiles at a high repetition rate, in order to minimize the effect of refraction. Due to cable length limitations, the MVP30 was only capable of sampling a fraction of the water depth, thus profiles had to be vertically extended in post-processing using archived sound speeds from an archived database [Hughes Clarke et al, 2011]. As a result, the profiles could not be applied to the MBES during data collection, thus all data from the Squamish repetitive survey program had to be re-raytraced using the extended profiles [Hughes Clarke et al, 2011].

The research efforts involved differencing the repetitive surveys on a day to day basis in order to detect changes in sedimentation, thus if any bias was introduced at the scale of a decimetre or larger, the volume calculations would be skewed. Figure 17 is a difference map between original data as collected, and the data re-processed using the cone intersection algorithm. For this example the data was re-processed keeping all values constant to demonstrate that the co-location assumption introduces biases as large as 1m (mean bias 0.06 m, standard deviation 0.23 m). If re-raytracing were to be done using the current algorithm, the biases introduced by the co-located array assumption would have significant consequences on the volume calculations.

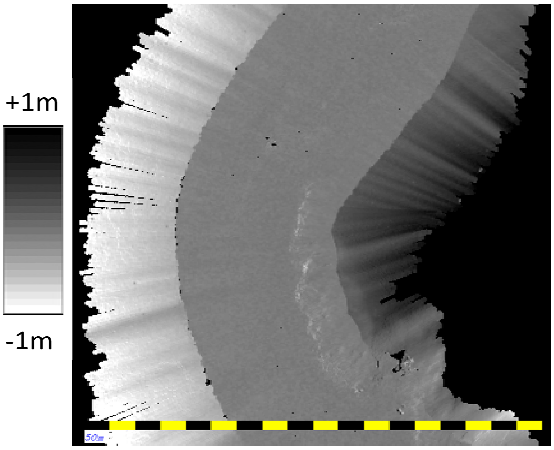

Figure 17: Difference map between original data as collected, and data reprocessed using the cone intersection algorithm. Differences represent the biases introduced by the co-location assumption.

Figure 18 is the same difference map, however the re-processing was done using the new algorithm. The mean bias created by the hyperbola intersection is 0.006 m with a standard deviation of 0.028 m. Any biases introduced by the new algorithm are small enough to be insignificant noise. As a result of using the new algorithm the accuracy of the volume estimations are now able to be improved by re-raytracing with the extended MVP30 sound speed casts.

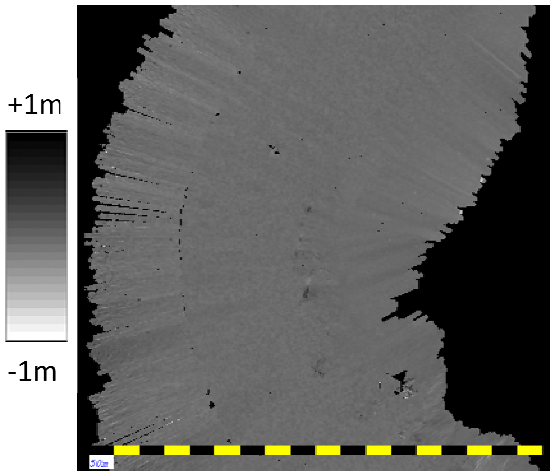

Figure 18: Difference map between original data as collected, and data reprocessed using the new algorithm. Differences represent the biases introduced by the hyperbola intersection assumption.

5 Conclusions

To address the biases created by the co-located array assumption in the commonly used cone intersection algorithm, a more precise algorithm has been developed that respects the true bi-static nature of the sonar configuration. The new method still contains its own assumptions; however in all tested datasets the biases caused by the hyperbola intersection are negligible when compared to the co-located array biases which it overcomes. Further work will be done to assure the biases remain negligible under all possible geometries.

By using the new algorithm, datasets which are collected with multi-sector systems that use yaw and pitch stabilization may now be corrected for erroneous or externally logged observations. Also developing this algorithm will help commercial software companies implement their own re-integration capabilities, helping to further progress processing capabilities throughout the hydrographic community.

References

Beaudoin, J., and J.E. Hughes Clarke (2004a). "Retracing (and re-raytracing) Amundsen's Journey through the Northwest Passage". *Proceedings of the Canadian Hydrographic Conference 2004*, Ottawa, Canada, CDROM.

Beaudoin, J., J.E. Hughes Clarke, and J. Bartlett (2004b). "Application of Surface Sound Speed Measurements in Post-Processing for Multi-Sector Multibeam Echosounders." *International Hydrographic Review*, v.5, no.3, p.26-31.

Bradie, B. (2006). *A Friendly Introduction to Numerical Analysis*. Pearson Prentice Hall, Upper Saddle River, New Jersey.

Hughes Clarke, J.E. (2012). "Optimal use of multibeam technology in the study of shelf Morphodynamics." *International Association of Sedimentologists*, Special Publication 44, p. 3-28.

Hughes Clarke, J.E., S. Brucker, J. Muggah, I. Church, D. Cartwright (2011). "The Squamish Delta Repetitive Survey Program: A simultaneous investigation of prodeltaic sedimentation and integrated system accuracy." *Proceedings of the U.S. Hydrographic Conference 2011*, Tampa, Florida, U.S.A..

Kongsberg (2006). *EM 3002*. Equipment Brochure, Horten, Norway.

Lurton, X. (2010). *An Introduction to Underwater Acoustics.* 2nd ed., Springer-Verlag, Berlin.